Bayesian inversion of frequency-domain airborne EM data with spatially correlation prior information

Jianmei Zhou, Dirk Husmeier, Hao Gao, Changchun Yin, Changkai Qiu, Xu Jing, Yanfu Qi and Wentao Liu

***Abstract*—Bayesian inversion of electromagnetic data can obtain key information on the uncertainty of subsurface resistivity. However, due to its high computational cost, Bayesian inversion is largely limited to 1D resistivity models. In this study, a fast Bayesian inversion method is implemented by introducing the spatial correlation as prior information. The contributions of this paper mainly include: (1) Explicitly introduce the expression of spatial correlation prior information, and provide a method to determine the parameters in the expression through the variogram theory. The influence of parameters in the spatial correlation prior information on the inversion results is systematically analyzed with 1D synthetic model. (2) The information entropy theory of continuous function is introduced to quantify the degrees of freedom of the parameters of the spatial correlation prior model. The analysis shows that the degree of freedom of model parameters is significantly smaller than the number of model parameters when spatial correlation prior information is introduced, which is the main reason for the rapid Bayesian inversion. (3) Introducing the sengpiel fast imaging algorithm, combined with the variogram theory, realized the direct acquisition of spatial correlation prior information from the observation data, minimizing the dependence on other information. The inversion results of 1D and 2D synthetic models and field dataset show that considering the spatial correlation prior information, hundreds of thousands of MCMC searches are needed to realize the inversion of up to thousands of model parameters. This result provides a possible idea for future Bayesian inversion of complex 3D models.**

***Index Terms*—airborne electromagnetic (AEM), statistical methods, Bayesian inversion, Markov chain Monte Carlo.**

I. Introduction

Frequency-domain airborne electromagnetic (AEM) methods are widely used in near-surface geophysical exploration [1-4]. AEM data interpretation mainly relies on inversion. For a review of various inversion methods for AEM data, refer to Yin *et al.* [5]. AEM inversion methods are mainly divided into deterministic inversion methods based on regularization theory and Bayesian inversion methods based on random sampling [5]. Deterministic inversion methods are based on various optimization methods to obtain a single inversion result [6-7], and has have been developed to the inversion of 3D model [8-10]. The Bayesian inversion method does not pursue a single inversion result, but obtains a model set that satisfies the observation information through random sampling, that is, the posterior distribution. Through posterior statistical analysis, the probability distribution and uncertainty information about the inversion results are provided [11]. Since uncertainty information can provide important references for subsequent geological interpretation, Bayesian inversion methods have received more and more attention in recent years [4,12-19].

The advantage disadvantage of the Bayesian inversion method is based on the increased computational cost. The deterministic inversion method generally only needs tens to hundreds of forward computations [8-10]. The Bayesian inversion method requires about 10^5~10^6 forward computations. This cost increase increases significantly with the increase of the dimension [11]. There are two main reasons. First, the calculation time of a single forward modeling increases as the dimension increases. The calculation time of a single frequency domain forward modeling of a 1D model only needs milliseconds [14]; while the single frequency domain forward modeling time of a 3D simple model needs more than seconds [20]. Second, the model parameters that need to be sampled increase exponentially as the dimension increases. Using the popular pixel parameterization strategy [21], the inversion parameters of the 1D model are generally tens to hundreds [6], while the inversion parameters of the 3D model are increased to tens of thousands [10].

In order to realize the Bayesian inversion of high-dimensional models, it is necessary to reduce the total inversion time as much as possible. One way is to increase the forward speed. Forward modeling acceleration can be achieved by improving the spatial grid discretization and governing equation solving methods [20,22]. Although these methods have made great progress, the forward time is still too long for Bayesian inversion [14]. In recent years, the development of machine learning [18] and model reduction [23] has the potential to greatly increase the speed of forward modeling, thereby enabling Bayesian inversion of high-dimensional models [23], which is an active research area.

Another way to reduce the total inversion time is to reduce the number of model parameters that need to be sampled. The pixel-based parameterization strategy can

This work was supported in part by the National Natural Science Foundation of China under Grant 42274092 and Grant 41830101, in part by the China Scholarship Council Foundation under Grant 202006565025, and in part by the Fundamental Research Funds for the Central Universities, CHD under Grant 300102261201. (Corresponding author: Jianmei Zhou.)

Jianmei Zhou is with the College of Geology Engineering and Geomatics, Chang'an University, Xi'an 710054, China, and also with the School of Mathematics and Statistics, University of Glasgow, Glasgow G12 8QQ, United Kingdom (e-mail: zhoujm@chd.edu.cn)

Dirk Husmeier and Hao Gao are with the School of Mathematics and Statistics, University of Glasgow, Glasgow G12 8QQ, United Kingdom (e-mail: Dirk.Husmeier@glasgow.ac.uk; Hao.Gao@glasgow.ac.uk)

Changchun Yin is with the College of Geo-Exploration Sciences and Technology, Jilin University, Changchun 130026, China (e-mail: yinchangchun@jlu.edu.cn)

Changkai Qiu is with the Development and Research Center, China Geological Survey, Beijing 100037, China (e-mail: qiuchangkai@hotmail.com)

Xu Jing, Yanfu Qi and Wentao Liu are with the College of Geology Engineering and Geomatics, Chang'an University, Xi'an 710054, China (e-mail: jx_tdem@chd.edu.cn; wtliu5369@163.com; jdqiyanfu@126.com).

easily represent various resistivity distributions, and the cost is that there is a large amount of parameter redundancy. Taking a 1D three-layer model as an example, the pixel-based parameterization is used to discretize it into 100 uniform thin layers, so the inversion model parameter is the resistivity of these 100 thin layers. Obviously, the 100 resistivity parameters of the three-layer model are not all truly independent. In fact, only 5 model parameters (2 formation thickness and 3 resistivity) are needed to fully describe the three-layer model. In actual inversion, the number of layers and the resistivity of each layer are unknown. Sampling can start with a half-space model that describes the fewest parameters, and gradually transition to a complex multi-layer model until it fits the observed data. This method can minimize the model parameters in the process of realizing the inversion. The widely popular trans-dimensional Markov chain Monte Carlo (MCMC) method [24-25] realizes this inversion process. This method is widely used in the probabilistic inversion of geophysical electromagnetic data, including 1D layered models [26-34] and 2D Voronoi cells [35-37]. However, this method is computationally complex and expensive when extended to 3D Voronoi cells [38-39].

From the view of the pixel-based parameterized model, the trans-dimensional MCMC method can be regarded as an algorithm that embeds the spatial correlation of model parameters into the sampling process. Both 1D layered model and 2D Voronoi unit can be regarded as the performance of strong spatial correlation. In order to avoid the difficulties of the trans-dimensional MCMC algorithm when it is extended to 3D Voronoi model, the spatial correlation of the model parameters can be explicitly added as prior information [40-42].

The effectiveness of Bayesian inversion depends on several factors, including the quality of the observed data, the accuracy of the forward algorithm and the rationality of the prior information. High quality observations correspond to low noise levels, and the observations are sensitive enough to the model parameters. High-precision forward algorithm is used to ensure that the inversion search model can have a good mapping relationship with the data. Reasonable and effective prior information can reduce the complexity of an inverse problem and that a prior with little information leads to a hard inverse problem [43]. Therefore, the selection of reasonable prior information is very important. The spatial correlation priori information, which holds that there is a correlation between the resistivity of the strata, can describe more realistic geological structure characteristics than the spatial uncorrelation priori information.

There are many forms of spatial correlation prior information, and a large class of methods that describe the spatial correlation of model parameters and the characteristics of more realistic geological structures are called geostatistical methods [44]. Bayesian inversion based on spatial correlation prior information has been applied in geophysics [4,14,40-42]. In particular, sequential Gibbs sampling [43] and the extended Metropolis algorithm [45] construct an inversion method that can use arbitrarily complex prior information [46-47]. This paper adopts the method of [46-47] to implement Bayesian inversion based on spatial correlation prior information.

Spatial correlation prior information affects the inversion results [48], so how to give prior information is important. Spatially correlated prior information generally requires deriving the statistical properties from borehole data or prior geological information about the study area [40–42]. In practice, this previous drilling or geological information may be lacking. To solve this problem, Hansen et al. [49] used the linearized stochastic inversion method to obtain spatial correlation prior information from observation data alone. The method determines the effectiveness of prior information selection by comparing the posterior probability density function with the prior probability density function. However, this method requires a large amount of model sampling to obtain spatially related prior information.

Compared with random prior information, spatial correlation prior information can reduce the degrees of freedom of inversion parameters [50], thereby reducing the complexity of probability inversion. But there is no clear quantitative description of how much the spatial correlation prior information reduces the degrees of freedom of the inversion parameters.

In this paper, we propose a new simple method to obtain the approximate spatial correlation prior information directly from the observational data. First, the sengpiel fast imaging algorithm [51] is introduced to obtain the apparent resistivity distribution of the underground model. Then we use the variogram theory to calculate the explicit variogram function of the model. Finally, the Gaussian spatial correlation prior model is obtained by fitting with the variogram model. The reasons for choosing the Gaussian model are as follows: AEM method is a diffuse field method. The observation data is based on the volume average of the electrical distribution in the subsurface. It naturally has a smoothing effect, so the subsurface model can be described by a Gaussian function [44] that also has a smoothing effect.

The spatial correlation prior model obtained by the above method is approximate. In order to analyze the impact of this approximation on the inversion results, we systematically discussed the relationship between the spatially related prior model parameters and the inversion results.

In addition, in order to better understand the impact of spatial correlation prior on the degree of freedom of model parameters, we introduced the information entropy theory [52] for quantitative analysis the reduction of the degrees of freedom of the parameters by the spatial correlation prior information.

The arrangement of this article is as follows: First, the forward modeling theory of frequency-domain AEM is briefly introduced. Next, the Bayesian inversion theory is introduced, emphasizing the spatial correlation prior information. Finally, the influence of parameters in the spatial correlation prior information on the inversion results is systematically analyzed with 1D synthetic model, and the inversion results of 2D synthetic models and field dataset are used to illustrate the potential of the algorithm in this paper in the Bayes inversion of high-dimensional models.

II. Forward Method

A. Model Parameterization

The frequency domain AEM method uses a loop source to transmitter primary magnetic fields of different frequencies. Based on the principle of electromagnetic induction, different secondary magnetic fields will be induced by earth models with different resistivity distributions. Another loop is used to receive the total magnetic field superimposed by the primary magnetic field and the secondary magnetic field. The subsurface resistivity distribution is inverted from the observed magnetic field data. In this paper, a unified pixel-based parameterization strategy is used to describe the geoelectric model in the process of forward modeling and inversion. For 1D problems, the subsurface resistivity distribution can be discretized into a layered model of *M* layers, and the layer thickness of each layer is fixed (generally selected as linear or logarithmic equidistant distribution). For 2D and 3D problems, the underground conductivity distribution can be discretized into a regular rectangular block model with a total of *M*, and the shape of each block is fixed (the horizontal direction generally adopts linear and equal interval distribution, and the vertical direction can choose linear or logarithmic equal interval distributed). The model parameters can be uniformly expressed as

$$\mathbf{m} = [m_1, m_2, \cdots, m_M] = [\log \rho_1, \log \rho_2, \cdots, \log \rho_M] \quad (1)$$

B. Forward Response

Due to the long calculation time of 2D and 3D forward modeling [20], this paper uniformly uses the 1D formula [12] to calculate the forward modeling response of the model. When the model is 2D, such as in sections 4.2 and 4.3, the electrical distribution directly below each measuring point is approximated as a 1D layered model to calculate the forward response of the measuring point. Due to the footprint effect [5], when the lateral electrical distribution of the measuring point area changes not particularly sharply, the forward modeling error of one-dimensional approximation is acceptable.

The transmitting coil and receiving coil of the frequency domain AEM method can adopt three kinds of geometrical devices [12]: horizontal coplanar (HCP), vertical coaxial (VCX) and vertical coplanar (VCP). The common one is the HCP device, which uses a horizontal coil to receive the vertical magnetic field transmitter by the vertical magnetic dipole source. The forward response in the 1D layered model can be expressed as [12]:

$$H_{zz} = \frac{q}{4\pi}\int_0^\infty \left[e^{-u_0(z+z_0)} + r_{TE}e^{u_0(z-z_0)}\right]\frac{\lambda^3}{u_0}J_0(\lambda L)d\lambda \quad (2)$$

Where q is the transmitting magnetic moment, z_0 is the height of the transmitting coil from the ground, L is the transmitting and receiving distance, r_{TE} is the reflection coefficient related to the model resistivity and layer thickness, and J_0 is the zero-order Bessel function. For forward responses of VCX and VCP systems, refer to [12]. The data used in frequency domain AEM data processing is the normalized secondary magnetic field:

$$d(\omega) = \frac{H_{zz}(\omega) - H_{zz}^0(\omega)}{H_{zz}^0(\omega)} \times 10^6 \quad (3)$$

where H_{zz} is the total field in equation (2), and H_{zz}^0 is the primary magnetic field. The forward modeling responses of equations (1)-(3) can be uniformly expressed as:

$$\mathbf{d} = g(\mathbf{m}) \quad (4)$$

where $\mathbf{d}$ is the forward response, and g is the nonlinear forward operator.

III. Inverse Method

In this paper, the Bayesian method [11] is used to solve the inverse problem. This method considers that all available information can be described by a probability density function (referred to as pdf), and solving the inverse problem is to combine the pdf of all known information. In a typical inverse problem, information can be described by prior information and a likelihood function.

A. Prior Information

Prior information represents a probabilistic representation of prior knowledge about the model, where prior knowledge can come from geological knowledge, previous geophysical exploration, etc. Before using prior information, it needs to be described quantitatively.

In the simplest case, assuming that all model parameters are mutually independent (i.e., spatially uncorrelated) and uniformly distributed within the parameter range $[m_{\min}, m_{\max}]$, the prior information can be expressed as [53]:

$$\pi_{pr}(m_i) = \begin{cases} 1/(m_{\max} - m_{\min}) & m_{\min} \le m_i \le m_{\max} \\ 0 & else \end{cases} \quad (5)$$

The spatially uncorrelated uniform distribution only gives the upper and lower limits of the variable range of parameters, contains the least prior information and the largest entropy, and corresponds to the largest degree of disorder. The spatially uncorrelated uniform distribution

described above is usually recommended if it is desired to minimize prior information [53]. Since the model parameters are spatially uncorrelated, the degrees of freedom of the model parameters are equal to the number of model parameters, $M_{free} = M$.

The spatially uncorrelated assumption can be convenient because its probability distribution values can be easily computed. However, such simple, spatially uncorrelated model parameters may not be a realistic description of the actually available information. The assumption of spatial uncorrelation means that two model parameters that are infinitely close together are assumed to be independent of each other. This assumption may often be inconsistent with most natural phenomena, since stratigraphic distributions may show highly correlated features. Many probability distributions exist that can describe spatially correlated model parameters and more realistic characterization of geological structures. One widely used class is the probability distribution model based on two-point Gaussian statistics [54]. The prior information is completely described by the mean and covariance between the model parameter pairs m_i and m_j , and m_i is normally distributed, then the prior information is a Gaussian distribution with mean $\mathbf{m}_0$ and covariance matrix $\mathbf{C}_M$ [54]:

$$\pi_{pr}(\mathbf{m} \mid \mathbf{m}_0, \mathbf{C}_M) = \frac{1}{\sqrt{(2\pi)^M |\mathbf{C}_M|}} \exp\left(-\frac{1}{2}(\mathbf{m}-\mathbf{m}_0)^{\mathrm{T}} \mathbf{C}_M^{-1} (\mathbf{m}-\mathbf{m}_0)\right) \quad (6)$$

Mean $\mathbf{m}_0$ corresponds to the average or background resistivity of the model. The spatial correlation covariance matrix $\mathbf{C}_M$ can be obtained by adding prior knowledge of the geostatistical properties of the subsurface. In geostatistical theory, spatial correlation models are generally described by variograms $\gamma(h)$. Commonly used variograms include spherical, exponential, and Gaussian models [54]. This paper adopts the Gaussian model. It is a smooth model. The variogram that specifically describes the gauss model is [54]:

$$\gamma(h) = c\left[1 - \exp\left(-\frac{3h^2}{r^2}\right)\right] \quad (7)$$

where h is the distance between the parameters m_i and m_j , r is the maximum correlation length, and c is the maximum value that the model parameters allow to change when h increases. Based on formula (7), the spatial correlation covariance matrix $\mathbf{C}_M$ can be obtained as:

$$\mathbf{C}_M = \begin{bmatrix} \gamma(0) & \gamma(1) & \cdots & \gamma(M) \\ \gamma(1) & \gamma(0) & \cdots & \gamma(M-1) \\ \vdots & \ddots & \ddots & \vdots \\ \gamma(M) & \cdots & \gamma(1) & \gamma(0) \end{bmatrix} \quad (8)$$

Spatial correlation prior information is generally unknown. How to obtain accurate spatially correlation prior information is an open topic. For areas with borehole data or existing geophysical information, the parameter mean and covariance matrix information of the spatial correlation prior model can be obtained through geostatistical analysis [55]. However, in many practical works, there is a lack of boreholes or existing geophysical information. In areas where only observation data exist, the acquisition of spatially correlated prior information may not be trivial [56-57].

This paper introduces the sengpiel fast imaging method [51] to obtain spatial correlation prior information, which can ensure the inversion effect without significantly increasing the amount of calculation. Firstly, an apparent resistivity distribution $\mathbf{m}_{ap}$ of the underground model is obtained by using the sengpiel fast imaging method [51]. Then the mean $\mathbf{m}_0$ can be obtained by the average of $\mathbf{m}_{ap}$. Apply the variogram formula [43] to $\mathbf{m}_{ap}$, we obtain the variogram corresponding to the apparent resistivity model:

$$\gamma_c(h_c) = \frac{1}{2N(h_c)} \sum_{i=1}^{N(h_c)} \left[m(x_i + h_c) - m(x_i)\right]^2 \quad (9)$$

here $m(x_i)$ is the value of model parameter at position x_i , h_c is the distance in the specified direction between spatial points $(x_i + h_c)$ and x_i , and $N(h_c)$ is the number of data pairs whose distance is h_c . $\gamma_c(h_c)$ is somewhat different from the theoretical Gaussian model $\gamma(h)$. We use the curve fitting method to obtain the corresponding Gaussian model $\gamma(h)$, and the covariance matrix $\mathbf{C}_m$ is then obtained according to formula (8).

$\gamma_c(h_c)$ is a variogram calculated based on the underground resistivity distribution. $\gamma_c(h_c)$ does not contain spatial correlation constraints, so the prior model obtained based on formula (8) of $\gamma_c(h_c)$ will not reduce the spatial degree of freedom of the model. This paper introduces the Gaussian spatial correlation prior constraint of formula (7). That is to say, $\gamma_c(h_c)$ can be fitted by $\gamma(h)$ with appropriate parameters. Therefore, $\gamma(h)$ is used instead of $\gamma_c(h_c)$ in the prior model. This constraint reduces the variation range of variograms, the degrees of freedom of model parameters will be much smaller than the number of model parameters [51].

B. *Degrees of Freedom of Prior Model*

By calculating the information entropy of the multivariate Gaussian distribution, the degrees of freedom of the parameters in the prior information can be quantitatively analyzed [58]. Since the model parameter $\mathbf{m}$ (i.e., the logarithmic conductivity) is a continuous

variable, it is necessary to use the information entropy formula of continuous random variables [58]:

$$\mathrm{I}(\mathbf{m}) = -\int_{-\infty}^{+\infty} \pi_{pr}(\mathbf{m}) \log \pi_{pr}(\mathbf{m}) d\mathbf{m} \tag{10}$$

Putting equation (6) into (10), the information entropy of the spatially correlated multivariate Gaussian distribution is as follows [58]:

$$\mathrm{I}(\mathbf{m} \mid \mathbf{m}_0, \mathbf{C}_m) = \frac{M}{2}(1 + \log 2\pi) + \frac{1}{2}\log|\mathbf{C}_m| \tag{11}$$

The information entropy of continuous variables can be positive or negative, but there are upper and lower limits [58]. Considering spatial correlation, when all model parameters are uncorrelated, it corresponds to the maximum entropy $\mathrm{I}_{\max}$; when all model parameters are spatially correlated, that is, the maximum correlation length is equal to the number of parameters $r = M$, corresponding to the minimum entropy $\mathrm{I}_{\min}$. Referring to the definition of the degree of freedom of the discrete parameter model [52], the degrees of freedom of the continuous parameter model corresponding to different r can be defined:

$$M_{free} = M \frac{\mathrm{I}(r) - \mathrm{I}_{\min}}{\mathrm{I}_{\max} - \mathrm{I}_{\min}} \tag{12}$$

Where $\mathrm{I}(r)$ is the information entropy of a given r. Obviously, when $M_{free} = M$, the model parameters are completely uncorrelated; and when $M_{free} = 0$, the model parameters are completely correlated. In practice, the spatial correlation of some model parameters is considered, that is, $0 < r < M$, the degrees of freedom of the corresponding model satisfy $0 < M_{free} < M$.

C. Likelihood Function

The likelihood function represents a probability measure of how well the forward response $g(\mathbf{m})$ of a given model $\mathbf{m}$ matches the observed data $\mathbf{d}^{obs}$. The likelihood function is [11]:

$$\pi_{like}(\mathbf{m}) = \int_D d\mathbf{d} \frac{\rho_D(g(\mathbf{m}))\theta(\mathbf{d} \mid \mathbf{m})}{\mu_D(\mathbf{d})} \tag{13}$$

where $\rho_D(g(\mathbf{m}))$ describes the measurement uncertainty. $\theta(\mathbf{d} \mid \mathbf{m})$ describes the model error, that is, the error caused by using imprecise forward operators g or imprecise model parameterization. $\mu_D(\mathbf{d})$ describes a homogeneous state of information, ensuring that the parameterizations in different coordinate systems are consistent. It is generally assumed that $\mu_D(\mathbf{d})$ can be approximated by a constant [53], while ignoring the error of the forward operator, the corresponding likelihood function can be simplified as [53]:

$$\pi_{like}(\mathbf{m}) = \rho_D(g(\mathbf{m})) \tag{14}$$

For the frequency-domain AEM method, it is assumed that the data noise is independent uncorrelated zero-mean Gaussian noise, and the standard deviation of the noise is 5ppm plus 5% of the observed data value, $\sigma_{d_i} = \sqrt{(0.05 \times d_i)^2 + 5^2}$. For N observed data, the corresponding likelihood function is expressed as [14]:

$$\pi_{like}(\mathbf{m}) = \prod_{i=1}^{N} \exp\left(-0.5 \frac{(d_{i_{obs}} - d_i(\mathbf{m}))^2}{\sigma_{d_i}^2} \right) \tag{15}$$

In the field of geophysical electromagnetics, a more intuitive data root mean square error (rms) is often used to view the fit of the inversion results:

$$\mathrm{rms} = \frac{1}{N} \sum_{i=1}^{N} \left(\frac{(d_{i_{obs}} - d_i(\mathbf{m}))^2}{\sigma_{d_i}^2} \right) \tag{16}$$

Ideally the inversion results are a perfect fit, corresponding to rms = 1.

D. Extended Metropolis Sampling Algorithm

Once the available information has been quantified, the concept of information state combination can be used to obtain the combined state of the information (prior distribution and likelihood), which leads to the posterior probability distribution [11]:

$$\pi_{post}(\mathbf{m}) = k \pi_{pr}(\mathbf{m}) \pi_{like}(\mathbf{m}) \tag{17}$$

where k is a normalization constant. Since the forward operator in equation (4) is a nonlinear operator, the posterior pdf cannot be directly obtained through equation (17). A common approach is to derive the posterior pdf based on sampling techniques. In order to evaluate equation (17), the classic Metropolis algorithm [59-60] needs to solve the prior probabilities and posterior probabilities at each sampling. Mosegaard and Tarantola proposed the extended Metropolis algorithm [45]. The algorithm does not need to solve the prior probability and posterior probability for every sampling, but only needs to solve the likelihood function, thereby reducing the calculate cost. More importantly, the algorithm allows in principle to include prior information with arbitrarily complex. The extended Metropolis algorithm is as follows [45]:

1. Near the existing model $\mathbf{m}_{cur}$, generate a candidate model $\mathbf{m}_{pro}$, which is consistent with the prior information.
2. Compute the likelihood function $\pi_{like}(\mathbf{m}_{pro})$ and acceptance probability of the candidate model $P_{acc} = \min\left(1, \frac{\pi_{like}(\mathbf{m}_{pro})}{\pi_{like}(\mathbf{m}_{cur})}\right)$.
3. If the candidate model is accepted, then $\mathbf{m}_{cur} = \mathbf{m}_{pro}$; if the candidate model is not accepted, then $\mathbf{m}_{cur}$ remain unchanged.
4. Go back to step 1 and continue to walk randomly around $\mathbf{m}_{cur}$.

There are only two requirements to run the above extended Metropolis algorithm. First, the likelihood function of the

candidate model $\pi_{like}(\mathbf{m}_{pro})$ can be calculated, as shown in equation (15), which is easy to implement, only the forward response of the candidate model needs to be calculated when solving. Second, the ability to efficiently sample the prior pdf enables step 1 in the algorithm. The Fast Fourier Transform Moving Average Method (FFTMA) provides an efficient way to sample spatially correlated multivariate Gaussian prior models [61], ensuring aperiodicity and irreducibility, for Multivariate Gaussian model generation is unconditionally realized efficiently. The specific principle is as follows. The m dimensional spatial correlation covariance matrix $\mathbf{C}_m$ can be expressed as a convolution of a matrix $\mathbf{s}$ and its transpose $\breve{\mathbf{s}}(x)=\mathbf{s}(-x)$:

$$\mathbf{C}_m=\mathbf{s}*\breve{\mathbf{s}} \tag{18}$$

If $\mathbf{s}$ can be calculated, the random model satisfying the mean $\mathbf{m}_0$ and the covariance matrix $\mathbf{C}_m$ can be expressed as:

$$\mathbf{m}=\mathbf{m}_0+\mathbf{s}*\mathbf{z} \tag{19}$$

where $\mathbf{z}$ is an m dimensional uncorrelated normal deviated field. In order to solve the time-consuming difficulty of calculating equation (18) when the dimension of C is large, Le Ravalec et al. proposed to transform the convolution calculation in equation (19) into Fourier space to achieve its fast solution [61]. The advantage of this method is that the spatial structure parameters (mean, covariance) and the random $\mathbf{z}$ are decoupled, so only changing the random $\mathbf{z}$ can produce different realizations with the same spatial structure parameters.

E. Gelman-Rubin Convergence Diagnostic

One critical question that MCMC practitioners need to address is when to stop the simulation. Roy reviews and discusses the most widely used MCMC convergence diagnostic tools [62]. In this paper, we use the Gelman-Rubin (GR) convergence diagnostic [63-64], which appears to be the most popular method for assessing samples [62]. Multiple chains were run in parallel with different random initial models, and sampling models from the burn-in period were excluded. Then it takes each of these chains and split into the first and second half. Let *mp* be the number of chains and *np* be the length of each chain. In this paper, we simulate 4 chains for all test model, each of length *nt*, and discard the 10% of *nt* as burn-in, so *mp* = 8 and *np* = 0.45*nt*.

For each model parameter estimand m_i, it labels the simulations as $m_i^{kj}(k=1,\cdots,np;j=1,\cdots,mp)$, and compute the between-sequence variances B and within-sequence variances W:

$$B=\frac{np}{mp-1}\sum_{j=1}^{mp}\left(\bar{m}_i^{\cdot j}-\bar{m}_i^{\cdot\cdot}\right)^2 \tag{20}$$

$$W=\frac{1}{mp(np-1)}\sum_{j=1}^{mp}\sum_{k=1}^{np}\left(m_i^{kj}-\bar{m}_i^{\cdot j}\right)^2 \tag{21}$$

where $\bar{m}_i^{\cdot j}=\frac{1}{np}\sum_{k=1}^{np}m_i^{kj}$ and $\bar{m}_i^{\cdot\cdot}=\frac{1}{mp}\sum_{j=1}^{mp}\bar{m}_i^{\cdot j}$. And the marginal posterior variance of the estimand *var* is estimate by *W* and *B*:

$$var=\frac{np-1}{np}W+\frac{1}{np}B \tag{22}$$

Then the potential scale reduction factor (PSRF) is estimating for monitor convergence of the simulation:

$$R=\sqrt{\frac{\text{var}}{W}} \tag{23}$$

which declines to 1 as $np\to\infty$. Gelman & Rubin [63] argue that the numerator in formula 23 overestimates var and underestimates *W*, making *R*>1. Simulation is stopped when *R* is sufficiently close to one. In this paper we use the cutoff value 1.1, which is generally used by MCMC practitioners [64].

IV. Numerical experiments

First, the 1D synthetic model is used to verify the improvement of the spatial correlation prior model on inversion results. The degrees of freedom of model parameters of spatial correlation prior information are quantitatively analyzed by using information entropy. The influence of imprecise spatial correlation information on Bayesian inversion results is discussed in detail. And introduce the Sengpiel imaging algorithm combined with the variogram formula to obtain the spatial correlation prior information and inversion results. Then the algorithm is extended to the inversion of 2D synthetic models to illustrate the feasibility of the algorithm for inversion of high-dimensional models. Finally, through the inversion of the field data and the comparison with the deterministic inversion results, the effectiveness of the algorithm in the actual data processing is illustrated. All the experiments were implemented on a laptop with 64G memory and 2.3GHz CPU i7-11800H.

A. 1D model

A 1D three-layer media model [65] is adopted, as shown in Fig. 1. The first layer is a high-resistance layer with a thickness of 25m and a resistivity of $200\,\Omega\cdot\mathrm{m}$; the second layer is a low-resistance layer with a thickness of 20m and a resistivity of $20\,\Omega\cdot\mathrm{m}$; the third layer is a high-resistance substrate with a resistivity of $500\,\Omega\cdot\mathrm{m}$. Using the HCP geometric device, the distance between the transmitter and the receiver is 8m, and the height of the transmitter from the ground is 30m. Calculate the vertical magnetic field for 5 typical frequencies (320Hz, 1500Hz, 6800Hz, 22000Hz and 100000Hz). Add 5% Gaussian random noise to the theoretical data as the inverted observation data, as shown in Figure 2.

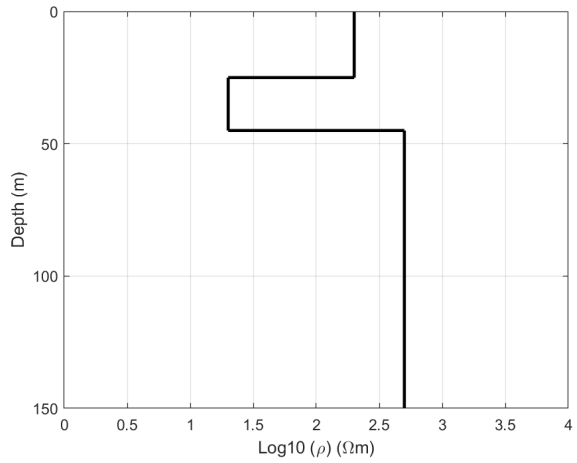

Fig.1 1D model

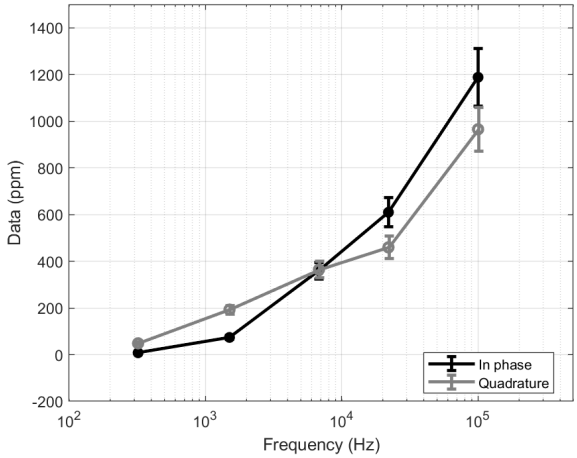

Fig.2 data of 1D model

The model needs to be parameterized before inversion. In this paper, the pixel-based parameterization method is used to discretize the model into linear and equally spaced thin layers with a layer number of M = 150 and a thickness of 1m.

Using a spatially uncorrelated prior model, all model parameters are independent of each other and uniformly distributed within the parameter range $[m_{\min}, m_{\max}]$, where $m_{\min} = 0.1\,\Omega\cdot\mathrm{m}$, $m_{\max} = 10000\,\Omega\cdot\mathrm{m}$, allowing the resistivity to vary continuously. Then the degrees of freedom of the model parameters are equal to the number of model parameters, $M_{free} = M$.

To adopt the spatial correlation prior model, the parameter information of the prior model needs to be given first. Knowing the real model as shown in Figure 1, the real spatial correlation information can be obtained. The model mean is set to the mean value of the formation logarithmic resistivity, m0 = 2.4479. The parameters r and c of the Gaussian variogram can be obtained by fitting the variogram. The variogram of the 1D model is calculated by equation (9), as shown by the black dotted line in Figure 3. The Gaussian variogram of equation (7) is used for fitting, as shown by the black solid line in Figure 3. It can be obtained that the parameters of the Gaussian variogram corresponding to the 1D model shown in Figure 1 are r = 25, c = 0.25.

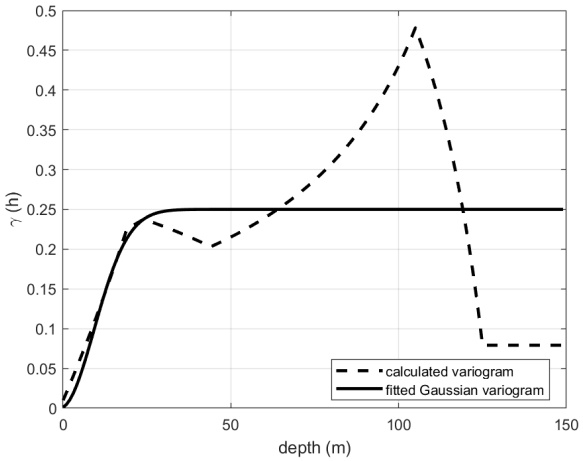

Fig.3 The calculated variogram (black dotted line) and the fitted Gaussian model variogram (black solid line) of the 1D model

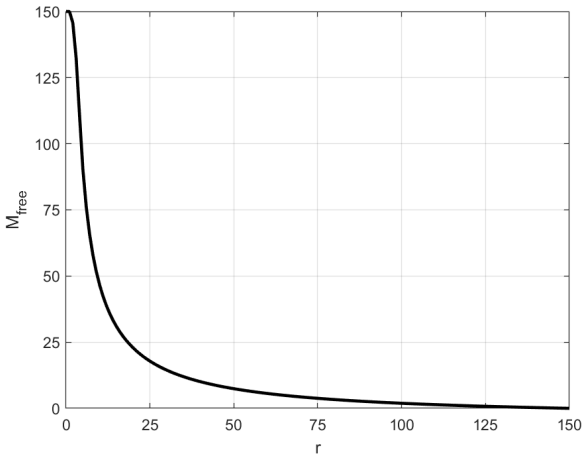

Fig.4 DOF of model parameter M_{free} corresponding to correlation length r

For the spatial correlation Gaussian model, the information entropy formulas (11) and (12) can be used to quantitatively analyze the degrees of freedom of the model parameters. Figure 4 shows the degrees of freedom corresponding to different correlation lengths r. As the correlation length r increases, the degrees of freedom of the model parameters decrease rapidly. When r = 0, $M_{free} = M$, the model is simplified to a spatially uncorrelated model; when r = 25, $M_{free} = 18$, the degrees of freedom are reduced to 12% of the number of model parameters. Bayesian inversion is a global search of the entire model space. The degree of freedom of the model parameters is reduced, which is equivalent to the reduction

of the search space of the model. When using the same number of searches, more efficient inversion results can thus be obtained.

The spatially uncorrelated prior model of formula (5) and the spatially correlated prior model of formula (6) are used for inversion respectively. The random prior models of spatial uncorrelation and spatial correlation are shown in Figure 5. Each parameter of the spatial uncorrelated model is randomly distributed within the parameter range, while the spatial correlation model has spatial continuity. Inversion iterative search 200,000 times. The convergence curve of the rms of the inversion data with the number of samples is shown in Figure 6. The inversion using the spatially correlated stochastic prior models converge to a stable distribution with rms of about 1, while inversion using the spatially uncorrelated prior models converge to a stable distribution with rms slightly greater than 1. Figure 7 shows the potential scale reduction factor R for model parameters with 200,000 sampling of spatially uncorrelated prior model (red) and spatially correlated prior model (green). R values of all model parameters are less than 1.1. According to the GR convergence diagnostic [64], we can consider that the MCMC search has converged. The R values of the inversion parameters of the spatially uncorrelated prior model are approximately randomly distributed. The R values of the inversion parameters of the spatially correlated prior model shows spatial correlation. The R value is larger near the interface where the model parameters change drastically.

Figure 8 shows the marginal posterior pdf of two different prior models. The probability density increases as the color deepens, and the middle area of the two green dotted lines is the 95% confidence interval. The solid green line is the posterior mean distribution, and the solid red line is the true model. Figure 8a is the inversion result of the spatially uncorrelated random prior model. The distribution of the posterior mean value is weakly reflected in the middle low-resistivity layer, but the range of the 95% confidence interval is too large to provide effective information about the distribution of model parameters. Figure 8b is the inversion result of the spatially correlated random prior model, and the overall curve of the posterior mean distribution is smooth, which is similar to the deterministic smooth constraint inversion result [6]. The posterior mean distribution clearly shows the existence and position information of the low-resistivity layer, and effectively presents the upper high-resistance layer and the lower layer. The 95% confidence interval reflects the uncertainty information of the inversion results. The 95% confidence intervals of the upper high-resistivity layer and the middle low-resistivity layer are relatively narrow, indicating that the uncertainty of the inversion results is small. The 95% confidence interval of the lower basement layer is relatively wide, indicating that the uncertainty of the inversion results is large.

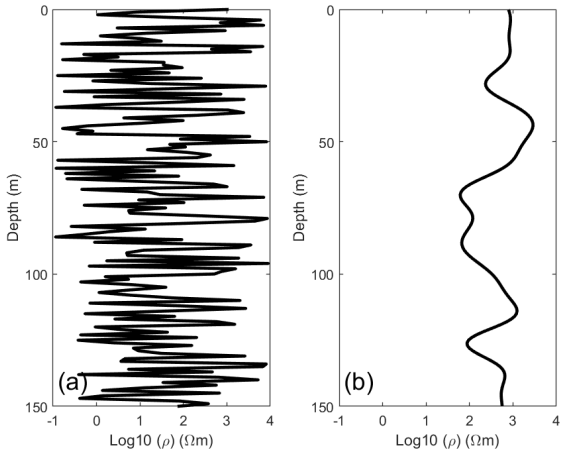

Fig.5 prior model. (a) Spatially uncorrelated prior model; (b) Spatially correlated prior model

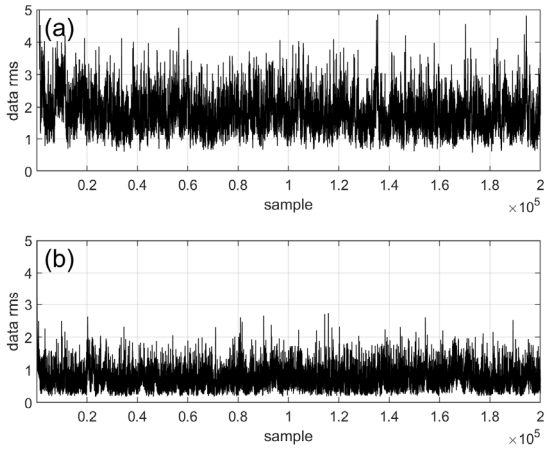

Fig.6 The data rms misfit convergence for sample. (a) Spatially uncorrelated prior model; (b) Spatially correlated prior model

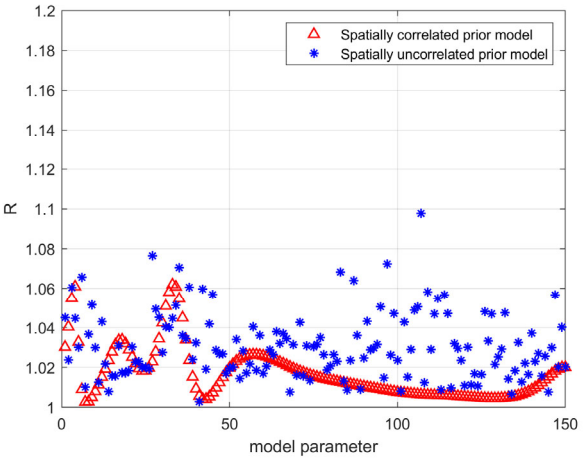

Fig.7 The potential scale reduction factor R for model parameters with 200,000 sampling of spatially uncorrelated prior model (red) and spatially correlated prior model (green)

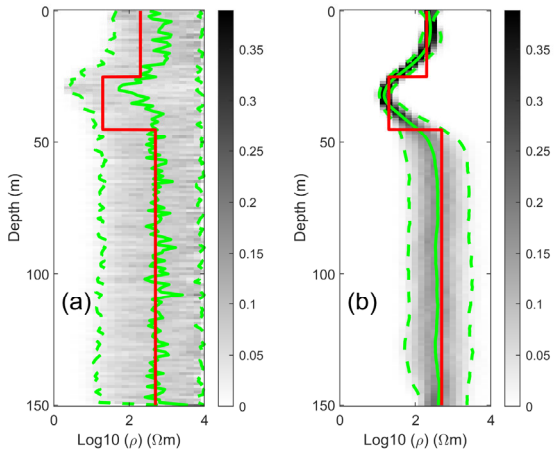

Fig.8 The posterior distribution of the 1D model inversion. (a) Spatially uncorrelated prior model; (b) Spatially correlated prior model

Using an accurate spatial correlation prior model, good inversion results can be obtained after the MCMC searches. However, it is difficult to obtain accurate spatial correlation prior model in practice. The influence of the inaccurate spatial correlation prior model on the inversion results is discussed below. Taking the three-layer model in Figure 1 as an example, it is assumed that there are only observation data and no other prior information. Taking the prior model parameters in Figure 3 as reference accurate values, that is, the model mean value m0 = 2.4479, corresponding to the average resistivity of 280 $\Omega\cdot$m, the parameter values of the Gaussian model variation function are r = 25, c = 0.25.

Figure 9 shows the inversion results of inaccurate m0, (a)-(d) are the inversion results of m0 as log10(100), log10(200), log10(350), and log10(500), respectively corresponding to the average resistivity of 100 $\Omega\cdot$m, 200 $\Omega\cdot$m, 350 $\Omega\cdot$m and 500 $\Omega\cdot$m. Comparing with Figure 8b, inaccurate m0 can still accurately invert the overburden and low-resistivity layer. The inaccurate m0 mainly affects the resistivity of the substrate high-resistivity layer. When m0 is too small, the inverted substrate resistivity is also too small, as shown in Figure 9a. when m0 is too large, the inverted substrate resistivity is also too large, as shown in Figure 9d.

Figure 10 shows the inversion results of inaccurate *r*, (a)-(d) are the inversion results of r being 5, 15, 25, and 35, respectively. Compared with Figure 8b, the inaccurate *r* mainly affects the smoothness of the formation curve. When *r* is smaller, the middle low-resistivity layer obtained by inversion is sharper, as shown in Fig. 10a, and the inversion formation curve is more oscillating. When *r* is too large, the middle low-resistivity layer obtained by inversion is smoother, and the inversion formation curve is smoother, as shown in Fig. 110d. The value of *r* reflects the knowledge of the minimum thickness of the formation.

Figure 11 shows the inversion results of inaccurate *c*, and (a)-(d) are the inversion results of *c* being 0.025, 0.1, 0.5, and 1, respectively. Compared with Figure 8b, the inaccurate c mainly affects the range of resistivity variation during the inversion process. When *c* is small, the allowable range of resistivity change in the inversion is small, so the inversion result is more concentrated (the range of the green dotted line is narrower), but when there is a large change in electrical properties, the inversion resistivity will deviate, as shown in the figure 11a, the inverted substrate resistivity is relatively small. As *c* increases, the allowable range of resistivity variation in the inversion gradually increases, and the inversion substrate resistivity gradually approaches the true resistivity, while the inversion results are more diffuse (the green dotted line has a wider range).

From Figure 9-11, it can be seen that the inaccurate spatial correlation prior information will affect the inversion results. When the spatial correlation prior model parameters deviate less than the real spatial correlation parameters of the model, the inversion results have little effect, such as (b) and (c) in Figure 8-10. When the spatial correlation prior parameters deviate significantly, it will have a significant impact on the inversion results.

In practice, we may only have observational data and lack prior information. In order to obtain the spatial correlation prior model, the sengpiel imaging method is firstly used to obtain the imaging model of electrical distribution, and the specific implementation process can refer to [63]. The imaging results are shown in Figure 12, and the sengpiel method can indicate the existence and approximate depth of the low-resistance layer. Then use formula (9) to calculate its variogram, and fit through formula (7) to obtain the spatial correlation prior model parameters, m0 = 2.0965, *r* = 35, and *c* = 0.04.

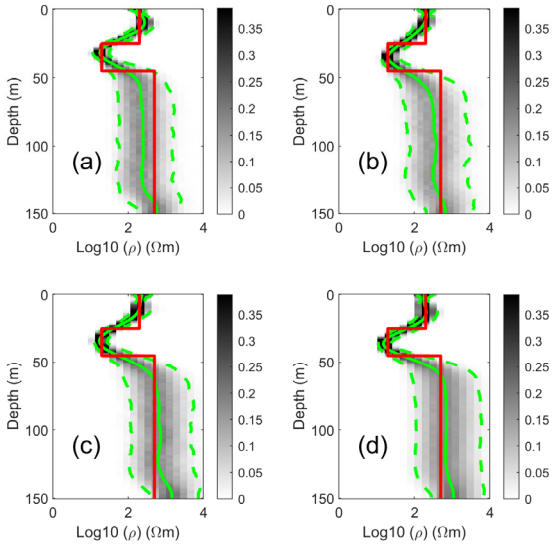

Fig.9 The posterior distribution of the 1D model inversion with inaccurate prior information. (a) m0=log10(100); (b) m0=log10(200); (c) m0=log10(350); (d) m0=log10(500).

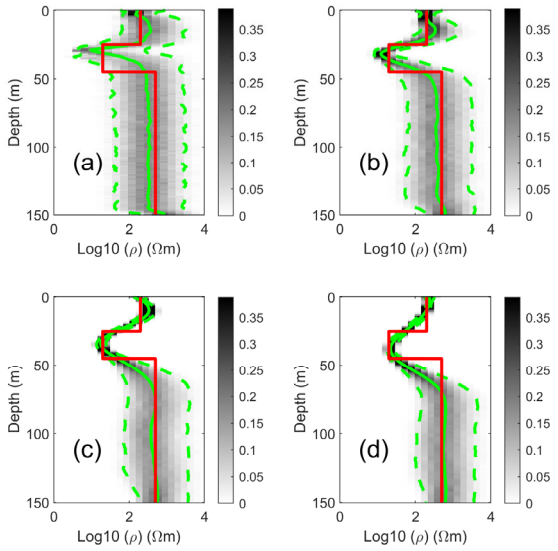

Fig.10 The posterior distribution of the 1D model inversion with inaccurate prior information. (a) r=5; (b) r=15; (c) r=35; (d) r=45.

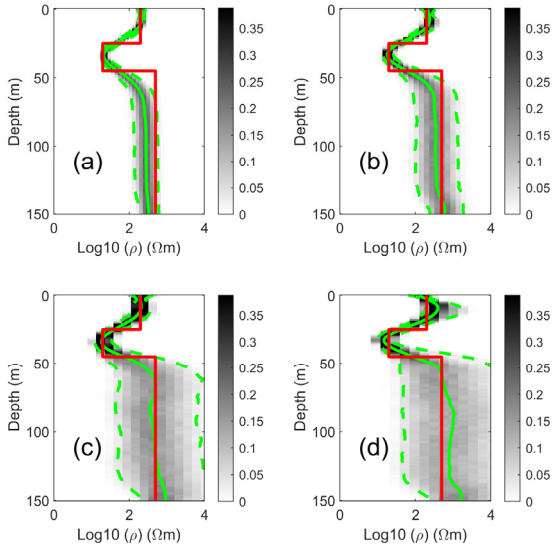

Fig.11 The posterior distribution of the 1D model inversion with inaccurate prior information. (a) c=0.025; (b) c=0.1; (c) c=0.5; (d) c=1.

Sengpiel imaging always tends to over smooth the resistivity of the model. Compared with the accurate spatial correlation prior parameters, m0 and *c* are relatively small, and *r* is relatively large. The posterior distribution with prior information from sengpiel result is shown in Figure 13a. This is the combined result of multiple model parameter inaccuracies. A small m0 results in a small substrate resistivity. A small value of *c* results in a small search range. A large *r* value causes the inversion curve to be too smooth. So, it is necessary to correct the spatial correlation prior model based on sengpiel imaging. Since the resistivity of basement are unknown, the correction of m0 may be processed in the opposite direction. In order to avoid such errors, we still keep m0 unchanged. The *r* obtained based on sengpiel imaging is always too large, and the obtained *c* is always too small. It is recommended to reduce *r* and increase *c* at the same time. A simple method is to reduce r and increase c by a factor, such as *r*/2 and 2*c*, then the corrected *r* =17.5, and *c* = 0.08. The inversion results based on the corrected spatial correlation prior model are shown in Figure 11b. The resistivity and position of the first layer and the second layer can be clearly inverted, but there is a certain difference in the substrate resistivity, which is caused by the small m0 in the prior information. We can also estimate *r* and *c* based on their physical meanings and geological understanding. For example, if we think that the thickness of the thinnest formation is 20m, and the resistivity contrast of the adjacent strata is twice, we can then choose *r*=20 and *c*=0.3. Obviously, a good understanding of geology can help to get more accurate *r* and *c*.

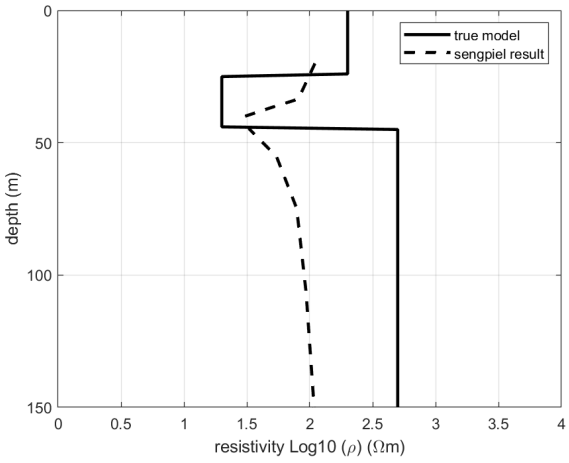

Fig.12 The sengpiel result of the 1D model.

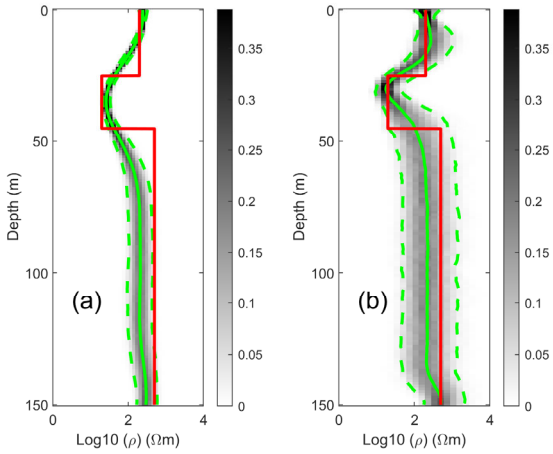

Fig.13 The sengpiel result (a) and the posterior distribution (b) with prior information from sengpiel result of the 1D model.

B. 2D model

Spatial correlation can significantly reduce the degrees of freedom of model parameters. This feature is more

prominent in the inversion of high-dimensional models. Consider a 2D wedge geoelectric model [63]. The length of the model along the horizontal direction is 100m; along the depth direction of the model, the first layer is a high-resistivity overburden with a thickness of 20m and a resistivity of $100\,\Omega\cdot\mathrm{m}$; the second layer is a low-resistivity wedge-shaped formation with a thickness gradually increasing from 8.9m to 24m and a resistivity of $20\,\Omega\cdot\mathrm{m}$; The third layer is a high-resistance substrate with a resistivity of $500\,\Omega\cdot\mathrm{m}$. Using the HCP geometric device, the distance between the transmitter and the receiver is 8m, and the height of the transmitter from the ground is 30m and the horizontal sampling interval is 20m, that is, the data of 6 measuring points are collected in total. Calculate the vertical magnetic field for 5 typical frequencies (320Hz, 1500Hz, 6800Hz, 22000Hz and 100000Hz). Add 5% Gaussian random noise to the theoretical data as the inverted observation data. During the inversion process, the forward response of each station is replaced by a 1D approximation of the stratigraphic distribution directly below the station. In numerical calculation, the wedge-shaped 2D model is approximated as a 2D model of step distribution, as shown in Figure 14. During the inversion of the model, the spatial discretization in the x and z directions is a uniform grid of 6×150, the inversion parameter is the resistivity of each uniform grid, and the number of model parameters is M = 900.

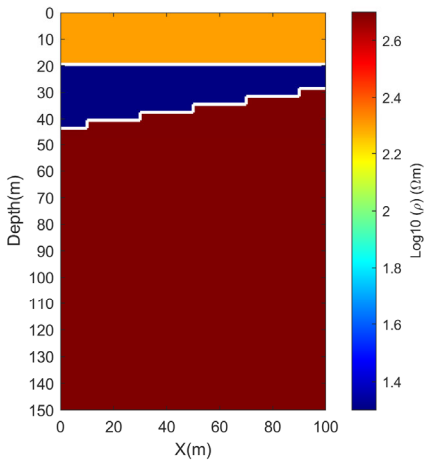

Fig.14 2D model

Spatially uncorrelated and spatially correlated prior models were used for inversion. When the spatially uncorrelated prior model is used, all model parameters are independent of each other and uniformly distributed within the parameter range $[m_{\min}, m_{\max}]$, where $m_{\min} = 0.1\,\Omega\cdot\mathrm{m}$, $m_{\max} = 10000\ \Omega\cdot\mathrm{m}$, allowing the resistivity to vary continuously. Degrees of freedom of the model parameters are equal to the number of model parameters, $M_{free} = M$.

When the spatial correlation prior model is used, the mean of the model is set to the average logarithmic resistivity, m0 = 2.4935. To solve the Gaussian variation function through the model Figure 15, it is necessary to extend the formula (9) to the 2D case, the variogram is calculated separately in the x direction and the z direction. For details, please refer to [54]. The results are shown in Figure 13, where the variograms in the x-direction and z-direction are shown by the black dotted line in the figure. The Gaussian model of formula 7 is used for fitting, as shown in the black solid line in Figure 15. The Gaussian variogram parameter of the 2D model are *rx*=5, *cx*=0.2, *rz*=20, *cz*=0.2.

For the spatially correlated Gaussian model, the maximum correlation length in *x* direction is 5, and in *z* direction is 20, so it can be considered that the maximum spatial correlation length of the 2D model is $r = 100$. The degrees of freedom of the parameters of the model are quantitatively analyzed using information entropy formulas. Figure 16 shows the degrees of freedom corresponding to different correlation lengths r. When $r = 0$, $M_{free} = M$, the model is simplified to a spatially uncorrelated model; when $r = 100$, $M_{free} = 32$, the degrees of freedom are reduced to 3.6% of the number of model parameters.

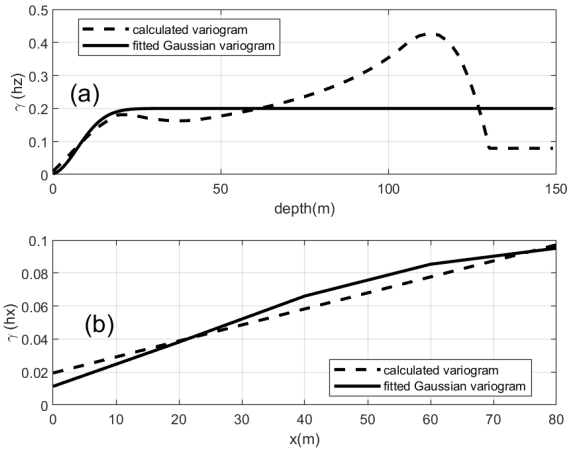

Fig.15 The calculated variogram (black dotted line) and the fitted Gaussian model variogram (black solid line) of the 2D model

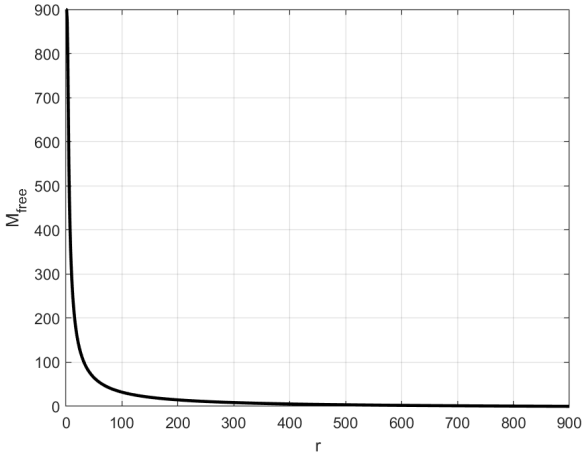

Fig.16 DOF corresponding to correlation length r of the 2D model

The spatially uncorrelated and the spatially correlated prior model are used for inversion respectively. Spatially uncorrelated and spatially correlated random prior models are shown in Figure 17. Each parameter of the spatially uncorrelated model is randomly distributed within the parameter range, while the spatially correlated model has spatial continuity.

Inversion iterative search 10^6 times. The convergence curve of the rms of the inversion data with the number of samples is shown in Figure 18. The inversion using the spatially correlated prior models converge to a stable distribution with rms of about 1, while inversion using the spatially uncorrelated prior models converge to a stable distribution with rms slightly greater than 1. Figure 19 shows the potential scale reduction factor R for model parameters with 10^6 sampling of spatially uncorrelated prior model (red) and spatially correlated prior model (green). Most model parameters have R-values less than 1.1, except for a few model parameters at the interface. This is similar to the R-value distribution of 1D model parameters.

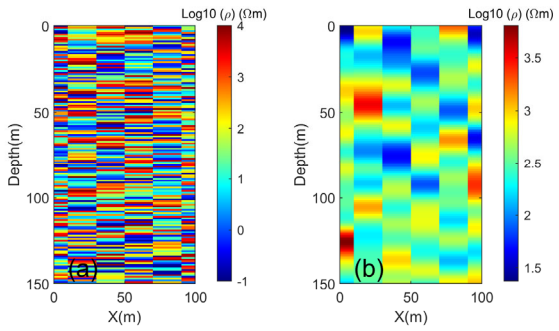

Fig.17 prior 2D model. (a) Spatially uncorrelated prior model; (b) Spatially correlated prior model

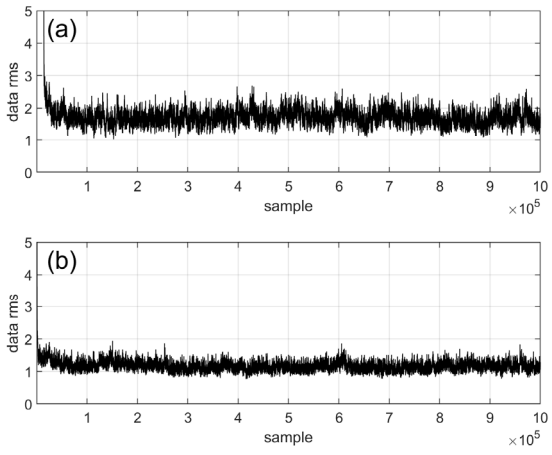

Fig.18 The data rms misfit convergence for sample. (a) Spatially uncorrelated prior model; (b) Spatially correlated prior model

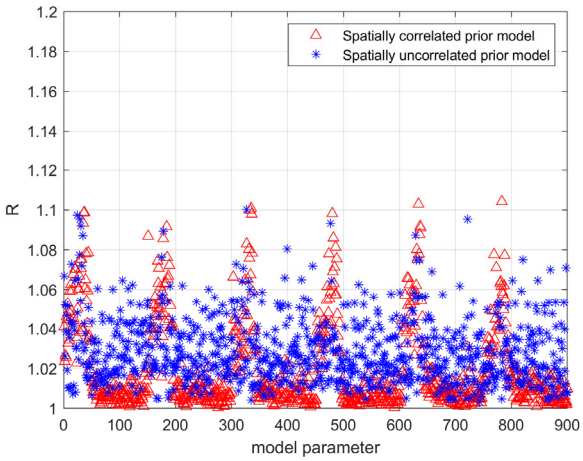

Fig.19 The data rms misfit convergence for sample. (a) Spatially uncorrelated prior model; (b) Spatially correlated prior model

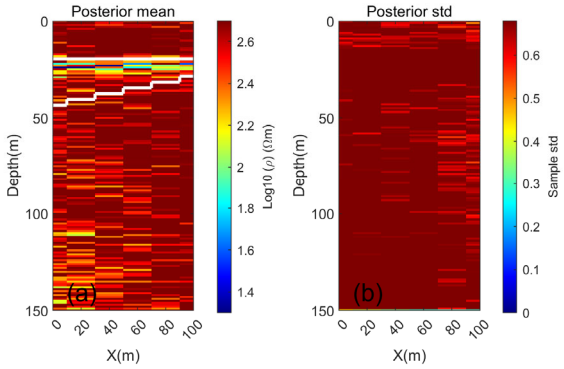

Fig.20 The posterior distribution of the 2D model based on spatially uncorrelated prior model. (a) posterior mean; (b) posterior standard deviation

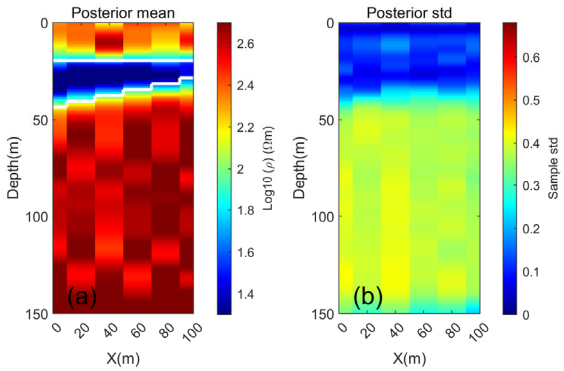

Fig.21 The posterior distribution of the 2D model based on spatially correlated prior model. (a) posterior mean; (b) posterior standard deviation

The inversion results using a spatially uncorrelated prior model are shown in Figure 20, the posterior distribution cannot provide effective information about the electrical distribution. The inversion results using the spatial correlation prior model are shown in Figure 21. Figure 21a is the posterior distribution mean. Compared with the model in Figure 14, the posterior distribution mean can well invert the distribution of underground electrical

properties, including the position of the layer interface and the resistivity value of the formation. Figure 21b shows the posterior standard deviation, which reflects the uncertainty of the inversion results. The uncertainty of the upper high-resistivity cover layer and the middle low-resistivity layer is small, while the uncertainty of the lower basement layer is large. This is consistent with the inversion results of the 1D model.

Considering the case where there are only observation data, we use the sengpiel imaging method to obtain the initial model of electrical distribution, as shown in Figure 22. The sengpiel method can indicate the presence and approximate depth of a low resistivity layer. Then we use formula (9) to calculate its variogram, and get the spatial correlation prior model parameters by fitting formula (7), m0 = 1.8594, rx = 10, cx = 0.04, rz = 80 and cz = 0.04. Due to the smoothing effect of sengpiel imaging, the spatially correlated prior model parameters in z direction always cause rz to be too large and cz to be too small. It is recommended to reduce the value of r and increase the value of c: rz = 40, cz =0.08. The inversion results based on the corrected spatial correlation prior information are shown in Fig. 23. Both the resistivity and formation position of the first layer and the second layer can be clearly inverted, but there is a certain difference in the substrate resistivity, which is caused by the small m0 in the prior information. This is consistent with the inversion results of the 1D model.

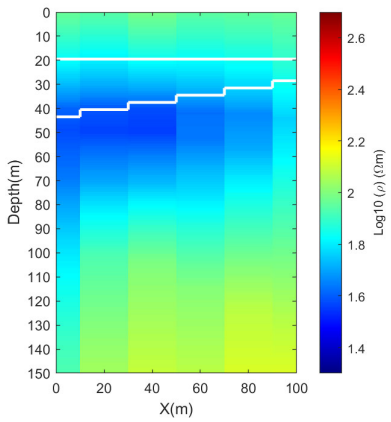

Fig.22 The sengpiel result of the 2D model

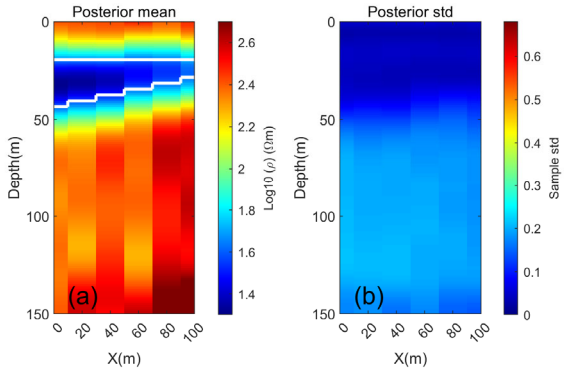

Fig.23 The posterior distribution of the 2D model with prior information from sengpiel results. (a) posterior mean; (b) posterior standard deviation

C. *Field data*

In order to verify the validity of the method proposed in this paper, the Bayesian inversion was performed on the field data of near-surface exploration in a certain place, and the inversion results were compared with the Occam inversion results. The field data are the vertical magnetic field components observed by the HCP geometry. The distance between the transmitter and the receiver is 7.9m, and the height of the transmitter from the ground is around 30m. The transmission frequencies are 386Hz, 1538Hz, 6257Hz, 25790Hz and 100264Hz. The horizontal length of the observation area is 500m, the distance between the measuring points is about 25m, and there are 21 observation points. Each observation point has 5 frequency data, and each data contains real part and imaginary part, so there are 210 data in total.

Figure 24 is the Occam inversion result. It can be seen from the figure that the formation of the entire section has good horizontal continuity, and the electrical distribution of the underground is roughly divided into three layers. The first layer is a high-resistivity layer with a thickness of about 10m, which is determined to be a sediment layer through field investigation. The second low-resistivity layer with a thickness of about 10m is determined to be a clay layer. The third layer is a high-resistivity basement, which is determined to be a sandy layer.

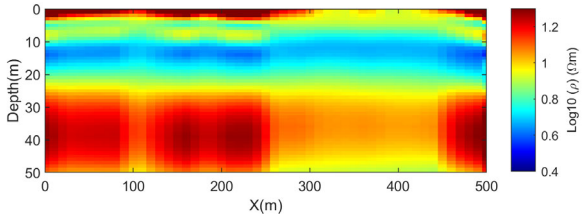

Fig.24 Inversion results of field data with Occam's method

Perform Bayesian inversion on field data. Firstly, the Sengpiel rapid imaging results are obtained through observation data, as shown in Figure 25. The sengpiel results indicated the existence and approximate buried depth of an intermediate low-resistivity. But the overall distribution is not clear enough.

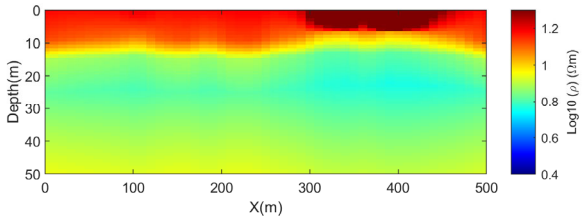

Fig.25 The sengpiel result of the field data

Next, spatial correlation prior information is obtained based on the sengpiel imaging results. According to the processing method of 1D and 2D models, formula (9) is used to calculate its variogram, and the spatial correlation prior model parameters are obtained by fitting formula (7), as shown in

Figure 26, and m0 = 0.9318, rx = 10, cx = 0.005, rz = 25 and cz = 0.04. Due to the smoothing effect of sengpiel imaging, it is recommended to reduce the value of r and increase the value of c: rz = 12.5, cz = 0.08. Due to the small resistivity m0, compared with the 1D and 2D models, the detection depth is reduced, and the maximum depth is set to 50m here. The detection area is spatially discretized, and the horizontal direction is separated according to the measuring point spacing, and the vertical direction is separated according to 1m equal intervals, so the number of model inversion parameters is M = 1050. The degrees of freedom of the parameters of the model are quantitatively analyzed using information entropy formulas. The total correlation length is $r = rx \times rz = 125$, then $M_{free} = 30$, the degrees of freedom are reduced to 2.9% of the number of model parameters.

The spatially correlated prior model is used for inversion. Inversion iterative search 10^6 times. The convergence curve of the rms of the inversion data with the number of samples is shown in Figure 27. The inversion with a spatially correlated prior model converged to a stationary distribution around rms = 1.5 after 15,000 searches. The potential scale reduction factor R is less than 1.1 for all the model parameters with 10^6 MCMC sampling.

The inversion results using the spatial correlation prior model are shown in Figure 28. Figure 28a is the posterior distribution mean. Compared with the Occam inverse result in Figure 24, the posterior distribution mean also gives a similar three-layer distribution, especially the low-resistance layer with good horizontal continuity. Figure 28b shows the posterior standard deviation, which reflects the uncertainty of the inversion results. Due to the shielding effect of the low-resistivity layer, the inversion results of formations below the low-resistivity layer are more uncertain than the inversion results above the low-resistivity layer.

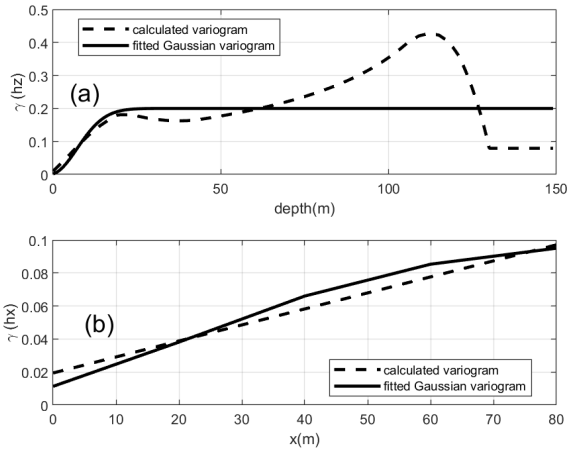

Fig.26 The calculated variogram (black dotted line) and the fitted Gaussian model variogram (black solid line) of the sengpiel result of field data

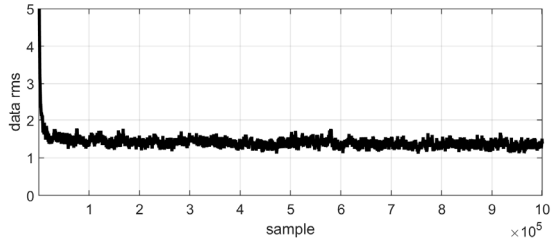

Fig.27 The data rms misfit convergence for sample for field data inversion.

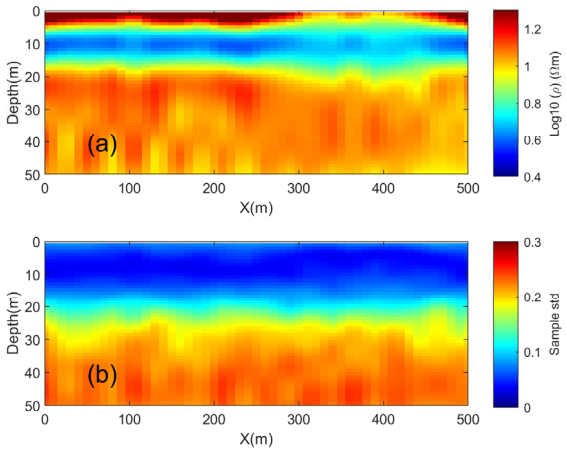

Fig.28 The posterior distribution of the field data with prior information from sengpiel results. (a) posterior mean; (b) posterior standard deviation

IV. Conclusion

This paper presents a Bayesian inversion method for frequency-domain airborne EM data. By explicitly adding spatially correlation prior information, the degree of freedom of model parameters is reduced, thereby improving the inversion effect and reducing time for inversion. The variogram theory is introduced to provide a method to determine the parameters in the spatial correlation prior information, and the influence of these parameters on the inversion results is discussed systematically. The analysis shows that the spatially correlated prior information allows a large dynamic range. Furthermore, in order to solve the practical problem of only observation data, and consider the influence characteristics of the spatial correlation prior model parameters on the inversion results, this paper introduces the sengpiel fast imaging algorithm combined with the variogram theory to provide spatial correlation prior information.

In order to have a quantitative understanding of the degree of freedom reduction of the spatial correlation prior model, the information entropy theory of continuous function is introduced to define the degrees of freedom of the spatial correlation model parameters. The calculation of the synthetic model shows that the parameter degree of freedom of the 1D model with the number of parameters M=150 is only 17.8, and the parameter degree of freedom of the 2D model with the number of parameters M=900 is only 32. The degree of freedom of model parameters will be significantly smaller than the number of model parameters by introducing spatial

correlation prior information, which provides the possibility for high-dimensional model inversion.

It should be noted that this paper only discusses the Gaussian variogram model. There are other more complex variograms in practice. In addition, this paper only obtains the spatial correlation prior model parameters by simply fitting the calculated variogram and Gaussian variogram, which is obviously not optimal. A more in-depth discussion of the above issues can be found in the detailed analysis in the field of Geostatistics [54]. For the case of only observational data, we employ the Sengpiel approximation imaging algorithm to provide spatially correlated prior information. Theoretically, it is possible to use the spatially correlated prior model parameters as inversion parameters and use a hierarchical model [66] to deal with it, but this may increase the amount of calculation and is not easy to implement, so we take it as a follow-up study. The Bayesian inversion in this paper only uses a single-chain search. In order to improve the inversion speed in the future, multi-chain parallelism can be considered. At the same time, in order to achieve a more effective search, the parallel tempering algorithm can be combined, for details, please refer to [67]. In this paper, when calculating 2D inversion, in order to reduce calculation time, forward modeling uses 1D approximation. In theory, it will lead to forward modeling errors, which need to be solved by forward modeling of high-dimensional models. However, the forward calculation of high-dimensional models is time-consuming. Therefore, for 3D probabilistic inversion, it is necessary to consider surrogate models or model reduction algorithms [23] to improve the forward calculation during the inversion process.

ACKNOWLEDGMENT

The authors would like to thank Prof. Thomas Mejer Hansen of Aarhus University for his guidance on spatial correlation prior information and information entropy theory and shared open-source code SIPPI. They would also like to thank Dr. Alan Lazarus of University of Glasgow for his guidance on MCMC theory. They would also like to thank associate Professor Lin Xin of Chang'an University for his guidance on variogram function. They would also like to thank associate Professor Ren Xiuyan of Jilin University for her guidance on Sengpiel imaging algorithm.

REFERENCES

[1] E. Auken, T. Boesen, and A. Christiansen, 'A Review of Airborne Electromagnetic Methods with Focus on Geotechnical and Hydrological Applications From 2007 to 2017', in Advances in Geophysics, 2017. doi: 10.1016/bs.agph.2017.10.002.

[2] B. J. Minsley, B. D. Smith, R. Hammack, J. I. Sams, and G. Veloski, 'Calibration and filtering strategies for frequency domain electromagnetic data', Journal of Applied Geophysics, vol. 80, pp. 56–66, May 2012, doi: 10.1016/j.jappgeo.2012.01.008.

[3] G. Hodges, E. Daly, L. Lafrenière, and Y. O'Connell, 'Environmental and geotechnical mapping with a fixed-wing frequency-domain electromagnetic system', Mar. 2016, pp. 17–20. doi: 10.4133/SAGEEP.29-004.

[4] D. Kiyan, V. Rath, M. R. Muller, M. D. Ture, and J. Hodgson, '1-D inversion of frequency-domain airborne electromagnetic data using the open-source aempy toolbox', Journal of Applied Geophysics, vol. 198, p. 104562, Mar. 2022, doi: https://doi.org/10.1016/j.jappgeo.2022.104562.

[5] Y. Chang-Chun, R. Xiu-Yan, L. Yun-He, Q. Yan-Fu, Q. Chang-Kai, and C. Jing, 'Review on airborne electromagnetic inverse theory and applications', GEOPHYSICS, vol. 80, no. 4, pp. W17–W31, Jul. 2015, doi: 10.1190/geo2014-0544.1.

[6] S. C. Constable, R. L. Parker, and C. G. Constable, 'Occam's inversion: A practical algorithm for generating smooth models from electromagnetic sounding data', Geophysics, vol. 52, no. 3, pp. 289–300, 1987.

[7] D. Fournier and D. W. Oldenburg, 'Inversion using spatially variable mixed ℓ p norms', Geophysical Journal International, vol. 218, no. 1, pp. 268–282, 2019.

[8] L. H. Cox, G. A. Wilson, and M. S. Zhdanov, '3D inversion of airborne electromagnetic data using a moving footprint', Exploration Geophysics, vol. 41, no. 4, pp. 250–259, Dec. 2010, doi: 10.1071/EG10003.

[9] Y. Liu, C. G. Farquharson, C. Yin, and V. C. Baranwal, 'Wavelet-based 3-D inversion for frequency-domain airborne EM data', Geophysical Journal International, vol. 213, no. 1, pp. 1–15, Apr. 2018, doi: 10.1093/gji/ggx545.

[10] B. Zhang, C. Yin, Y. Liu, X. Ren, V. C. Baranwal, and B. Xiong, '3D inversion of large-scale frequency-domain airborne electromagnetic data using unstructured local mesh', GEOPHYSICS, vol. 86, no. 5, pp. E333–E342, Sep. 2021, doi: 10.1190/geo2020-0243.1.

[11] A. Tarantola, Inverse Problem Theory and Methods for Model Parameter Estimation. in Other Titles in Applied Mathematics. Society for Industrial and Applied Mathematics, 2005. doi: 10.1137/1.9780898717921.

[12] B. J. Minsley, 'A trans-dimensional Bayesian Markov chain Monte Carlo algorithm for model assessment using frequency-domain electromagnetic data', Geophysical Journal International, vol. 187, no. 1, pp. 252–272, 2011, doi: 10.1111/j.1365-246X.2011.05165.x.

[13] J. R. Delsman et al., 'Large-scale, probabilistic salinity mapping using airborne electromagnetics for groundwater management in Zeeland, the Netherlands', Environ. Res. Lett., vol. 13, no. 8, p. 084011, Jul. 2018, doi: 10.1088/1748-9326/aad19e.

[14] T. M. Hansen and B. J. Minsley, 'Inversion of airborne EM data with an explicit choice of prior model', Geophysical Journal International, vol. 218, no. 2, pp. 1348–1366, 2019.

[15] C. Bobe, E. Van De Vijver, J. Keller, D. Hanssens, M. Van Meirvenne, and P. De Smedt, 'Probabilistic 1-D Inversion of Frequency-Domain Electromagnetic Data Using a Kalman Ensemble Generator', IEEE Transactions on Geoscience and Remote Sensing, vol. 58, no. 5, pp. 3287–3297, May 2020, doi: 10.1109/TGRS.2019.2953004.

[16] T. M. Hansen, 'Efficient probabilistic inversion using the rejection sampler—exemplified on airborne EM data', Geophysical Journal International, vol. 224, no. 1, pp. 543–557, Jan. 2021, doi: 10.1093/gji/ggaa491.

[17] B. J. Minsley, N. L. Foks, and P. A. Bedrosian, 'Quantifying model structural uncertainty using airborne electromagnetic data', Geophysical Journal International, vol. 224, no. 1, pp. 590–607, Jan. 2021, doi: 10.1093/gji/ggaa393.

[18] T. Hansen and C. Finlay, 'Use of machine learning to estimate statistics of the posterior distribution in probabilistic inverse problems - an application to airborne EM data.', Journal of Geophysical Research: Solid Earth, vol. 127, Oct. 2022, doi: 10.1029/2022JB024703.

[19] S. Wu, Q. Huang, and L. Zhao, 'Fast Bayesian Inversion of Airborne Electromagnetic Data Based on the Invertible Neural Network', IEEE Transactions on Geoscience and Remote Sensing, vol. 61, pp. 1–11, 2023, doi: 10.1109/TGRS.2023.3264777.

[20] X. Han et al., '3D Finite-Element Forward Modeling of Airborne EM Systems in Frequency-Domain Using Octree Meshes', IEEE Transactions on Geoscience and Remote Sensing, vol. 60, pp. 1–13, 2022, doi: 10.1109/TGRS.2022.3153026.

[21] A. Abubakar, T. M. Habashy, M. Li, and J. Liu, 'Inversion algorithms for large-scale geophysical electromagnetic measurements', Inverse Problems, vol. 25, no. 12, p. 123012, Dec. 2009, doi: 10.1088/0266-5611/25/12/123012.

[22] J. ZHOU, W. LIU, H. LIU, X. LI, and Z. QI, 'Research on rational Krylov subspace model order reduction algorithm for three-dimensional multi-frequency CSEM modelling', Chinese Journal of Geophysics, vol. 61, no. 6, pp. 2525–2536, 2018.

[23] M. C. Manassero, J. C. Afonso, F. Zyserman, S. Zlotnik, and I. Fomin, 'A reduced order approach for probabilistic inversions of 3-D magnetotelluric data I: general formulation', Geophysical Journal International, vol. 223, no. 3, pp. 1837–1863, Nov. 2020, doi: 10.1093/gji/ggaa415.

[24] P. J. Green, 'Reversible jump Markov chain monte carlo computation and Bayesian model determination', Biometrika, vol. 82, no. 4, pp. 711–732, 1995, doi: 10.1093/biomet/82.4.711.
[25] M. Sambridge, K. Gallagher, A. Jackson, and P. Rickwood, 'Trans-dimensional inverse problems, model comparison and the evidence', Geophysical Journal International, vol. 167, no. 2, pp. 528–542, Nov. 2006, doi: 10.1111/j.1365-246X.2006.03155.x.
[26] R. Brodie and M. Sambridge, 'Transdimensional Monte Carlo Inversion of AEM Data', ASEG Extended Abstracts, vol. 2012, Dec. 2012, doi: 10.1071/ASEG2012ab095.
[27] A. Ray and K. Key, 'Bayesian inversion of marine CSEM data with a trans-dimensional self parametrizing algorithm', Geophysical Journal International, vol. 191, no. 3, pp. 1135–1151, 2012, doi: 10.1111/j.1365-246X.2012.05677.x.
[28] A. Ray, D. L. Alumbaugh, G. Hoversten, and K. Key, 'Robust and accelerated Bayesian inversion of marine controlled-source electromagnetic data using parallel tempering', GEOPHYSICS, vol. 78, pp. 271-E280, 01 2013, doi: 10.1190/geo2013-0128.1.
[29] D. Blatter, K. Key, A. Ray, N. Foley, S. Tulaczyk, and E. Auken, 'Trans-dimensional Bayesian inversion of airborne transient EM data from Taylor Glacier, Antarctica', Geophysical Journal International, vol. 214, no. 3, pp. 1919–1936, 2018, doi: 10.1093/gji/ggy255.
[30] E. Mandolesi, X. Ogaya, J. Campanyà, and N. P. Agostinetti, 'A reversible-jump Markov chain Monte Carlo algorithm for 1D inversion of magnetotelluric data', Computers & Geosciences, vol. 113, pp. 94–105, 2018.
[31] E. Xiang, R. Guo, S. E. Dosso, J. Liu, H. Dong, and Z. Ren, 'Efficient hierarchical trans-dimensional Bayesian inversion of magnetotelluric data', Geophysical Journal International, vol. 213, no. 3, pp. 1751–1767, 2018, doi: 10.1093/gji/ggy071.
[32] A. Ray and D. Myer, 'Bayesian geophysical inversion with trans-dimensional Gaussian process machine learning', Geophysical Journal International, vol. 217, no. 3, pp. 1706–1726, 2019, doi: 10.1093/gji/ggz111.
[33] R. Peng, B. Han, X. Hu, J. Li, and Y. Liu, 'Transdimensional Bayesian inversion of magnetotelluric data in anisotropic layered media with galvanic distortion correction', Geophysical Journal International, vol. 228, no. 3, pp. 1494–1511, Mar. 2022, doi: 10.1093/gji/ggab413.
[34] H. Yao, Z. Ren, J. Tang, R. Guo, and J. Yan, 'Trans-dimensional Bayesian joint inversion of magnetotelluric and geomagnetic depth sounding responses to constrain mantle electrical discontinuities', Geophysical Journal International, vol. 233, no. 3, pp. 1821–1846, Jun. 2023, doi: 10.1093/gji/ggad029.
[35] E. Galetti and A. Curtis, 'Transdimensional electrical resistivity tomography', Journal of Geophysical Research: Solid Earth, vol. 123, no. 8, pp. 6347–6377, 2018.
[36] A. Ray, K. Key, T. Bodin, D. Myer, and S. Constable, 'Bayesian inversion of marine CSEM data from the Scarborough gas field using a transdimensional 2-D parametrization', Geophysical Journal International, vol. 199, no. 3, pp. 1847–1860, 2014.
[37] R. Hawkins, R. C. Brodie, and M. Sambridge, 'Trans-dimensional Bayesian inversion of airborne electromagnetic data for 2D conductivity profiles', Exploration Geophysics, vol. 49, no. 2, pp. 134–147, Apr. 2018, doi: 10.1071/EG16139.
[38] N. Piana Agostinetti, G. Giacomuzzi, and A. Malinverno, 'Local three-dimensional earthquake tomography by trans-dimensional Monte Carlo sampling', Geophysical Journal International, vol. 201, no. 3, pp. 1598–1617, Jun. 2015, doi: 10.1093/gji/ggv084.
[39] X. Zhang, A. Curtis, E. Galetti, and S. de Ridder, '3-D Monte Carlo surface wave tomography', Geophysical Journal International, vol. 215, no. 3, pp. 1644–1658, 2018.
[40] M. Aleardi, A. Vinciguerra, and A. Hojat, 'A geostatistical Markov chain Monte Carlo inversion algorithm for electrical resistivity tomography', Near Surface Geophysics, vol. 19, no. 1, pp. 7–26, 2021, doi: 10.1002/nsg.12133.
[41] D. Grana, L. de Figueiredo, and K. Mosegaard, 'Markov chain Monte Carlo for petrophysical inversion', Geophysics, vol. 87, no. 1, pp. M13–M24, Nov. 2022, doi: 10.1190/geo2021-0177.1.
[42] J. Narciso, C. Bobe, L. Azevedo, and E. Van De Vijver, 'A comparison between Kalman ensemble generator and geostatistical frequency-domain electromagnetic inversion: The impacts on near-surface characterization', Geophysics, vol. 87, no. 5, pp. E335–E346, Aug. 2022, doi: 10.1190/geo2021-0498.1.
[43] T. Hansen, K. Cordua, and K. Mosegaard, 'Inverse problems with non-trivial priors: Efficient solution through sequential Gibbs sampling', Computational Geosciences, vol. 16, Jun. 2012, doi: 10.1007/s10596-011-9271-1.
[44] S. Maroufpoor, O. Bozorg-Haddad, and X. Chu, 'Chapter 9 - Geostatistics: principles and methods', in Handbook of Probabilistic Models, P. Samui, D. Tien Bui, S. Chakraborty, and R. C. Deo, Eds., Butterworth-Heinemann, 2020, pp. 229–242. doi: 10.1016/B978-0-12-816514-0.00009-6.
[45] K. Mosegaard and A. Tarantola, 'Monte Carlo sampling of solutions to inverse problems', Journal of Geophysical Research: Solid Earth, vol. 100, no. B7, pp. 12431–12447, 1995, doi: 10.1029/94JB03097.
[46] T. Mejer Hansen, K. Skou Cordua, M. Caroline Looms, and K. Mosegaard, 'SIPPI: A Matlab toolbox for sampling the solution to inverse problems with complex prior information: Part 1—Methodology', Computers & Geosciences, vol. 52, pp. 470–480, Mar. 2013, doi: https://doi.org/10.1016/j.cageo.2012.09.004.
[47] T. M. Hansen, K. S. Cordua, M. C. Looms, and K. Mosegaard, 'SIPPI: A Matlab toolbox for sampling the solution to inverse problems with complex prior information: Part 2—Application to crosshole GPR tomography', Computers & Geosciences, vol. 52, pp. 481 – 492, Mar. 2013, doi: https://doi.org/10.1016/j.cageo.2012.10.001.
[48] K. S. Cordua, T. M. Hansen, and K. Mosegaard, 'Monte Carlo full-waveform inversion of crosshole GPR data using multiple-point geostatistical a priori information', Geophysics, vol. 77, no. 2, pp. H19–H31, Feb. 2012, doi: 10.1190/geo2011-0170.1.
[49] T. M. Hansen, M. C. Looms, and L. Nielsen, 'Inferring the Subsurface Structural Covariance Model Using Cross-Borehole Ground Penetrating Radar Tomography', Vadose Zone Journal, vol. 7, no. 1, pp. 249–262, 2008, doi: 10.2136/vzj2006.0144.
[50] T. Hansen, H. Klaus, M. Knud, and K. Cordua, 'Reducing complexity of inverse problems using geostatistical priors', Jan. 2009.
[51] D. C. Fraser, 'Resistivity mapping with an airborne multicoil electromagnetic system', Geophysics, vol. 43, no. 1, pp. 144–172, Feb. 1978, doi: 10.1190/1.1440817.
[52] T. M. Hansen, 'Entropy and Information Content of Geostatistical Models', Math Geosci, vol. 53, no. 1, pp. 163–184, Jan. 2021, doi: 10.1007/s11004-020-09876-z.
[53] T. M. Hansen, K. S. Cordua, A. Zunino, and K. Mosegaard, 'Probabilistic Integration of Geo-Information', in Geophysical Monograph Series, M. Moorkamp, P. G. Lelièvre, N. Linde, and A. Khan, Eds., Hoboken, NJ: John Wiley & Sons, Inc, 2016, pp. 93–116. doi: 10.1002/9781118929063.ch6.
[54] L. Azevedo and A. Soares, Geostatistical Methods for Reservoir Geophysics. in Advances in Oil and Gas Exploration & Production. Cham: Springer International Publishing, 2017. doi: 10.1007/978-3-319-53201-1.
[55] M. Bosch, 'Lithologic tomography: From plural geophysical data to lithology estimation', Journal of Geophysical Research: Solid Earth, vol. 104, no. B1, pp. 749–766, 1999, doi: 10.1029/1998JB900014.
[56] J. Irving, R. Knight, and K. Holliger, 'Estimation of the lateral correlation structure of subsurface water content from surface-based ground-penetrating radar reflection images', Water Resources Research, vol. 45, no. 12, 2009, doi: 10.1029/2008WR007471.
[57] M. Looms, T. Hansen, K. Cordua, L. Nielsen, K. Jensen, and A. Binley, 'Geostatistical inference using crosshole ground-penetrating radar', Geophysics, vol. 75, Nov. 2010, doi: 10.1190/1.3496001.
[58] T. M. Cover, Elements of information theory. John Wiley & Sons, 1999.
[59] N. Metropolis, A. W. Rosenbluth, M. N. Rosenbluth, A. H. Teller, and E. Teller, 'Equation of State Calculations by Fast Computing Machines', The Journal of Chemical Physics, vol. 21, no. 6, pp. 1087–1092, 1953, doi: 10.1063/1.1699114.
[60] W. K. Hastings, 'Monte Carlo sampling methods using Markov chains and their applications', Biometrika, vol. 57, no. 1, pp. 97–109, Apr. 1970, doi: 10.1093/biomet/57.1.97.
[61] M. L. Ravalec, B. Noetinger, and L. Y. Hu, 'The FFT Moving Average (FFT-MA) Generator: An Efficient Numerical Method for Generating and Conditioning Gaussian Simulations', Mathematical Geology, vol. 32, no. 6, pp. 701–723, Aug. 2000, doi: 10.1023/A:1007542406333.
[62] Roy, Vivekananda. 'Convergence Diagnostics for Markov Chain Monte Carlo', Annual Review of Statistics and Its Application, vol.7, no.1, pp 387 – 412, 2020. https://doi.org/10.1146/annurev-statistics-031219-041300.

[63] A. Gelman and D. B. Rubin, 'Inference from Iterative Simulation Using Multiple Sequences', Statistical Science, vol. 7, no. 4, pp. 457–472, Nov. 1992, doi: 10.1214/ss/1177011136.
[64] A. Gelman, J. B. Carlin, H. S. Stern, D. B. Dunson, A. Vehtari, D. B. Bayesian Data Analysis. Three Edition. New York: Chapman and Hall/CRC, 2015. https://doi.org/10.1201/b16018.
[65] C.Yin, Airborne electromagnetic theory and exploration technology. Science Press.2018
[66] G. M. Allenby, P. E. Rossi, and R. E. McCulloch, 'Hierarchical Bayes Models: A Practitioners Guide'. Rochester, NY, Jan. 01, 2005. doi: 10.2139/ssrn.655541.
[67] M. Sambridge, 'A parallel tempering algorithm for probabilistic sampling and multimodal optimization', Geophysical Journal International, vol. 196, no. 1, pp. 357–374, 2014.